

# Performance Assessment of Linear Models of Hydropower Plants

Stefano Cassano, Fabrizio Sossan  
PERSEE, Mines ParisTech - PSL  
Sophia Antipolis, France  
{stefano.cassano, fabrizio.sossan}@mines-paristech.fr

Christian Landry, Christophe Nicolet  
Power Vision Engineering Sarl  
St-Sulpice, Switzerland  
{christian.landry, christophe.nicolet}@powervision-eng.ch

**Abstract**—This paper discusses linearized models of hydropower plants (HPPs). First, it reviews state-of-the-art models and discusses their non-linearities, then it proposes suitable linearization strategies for the plant head, discharge, and turbine torque. It is shown that neglecting the dependency of the hydro-acoustic resistance on the discharge leads to a linear formulation of the hydraulic circuits model. For the turbine, a numerical linearization based on a first-order Taylor expansion is proposed. Model performance is evaluated for a medium- and a low-head HPP with a Francis and Kaplan turbine, respectively. Perspective applications of these linear models are in the context of efficient model predictive control of HPPs based on convex optimization.

**Index Terms**—Hydropower plants, Linear models, Model predictive control.

## I. INTRODUCTION

Hydropower plants (HPPs) are a key renewable generation asset, covering more than 10% of the electricity needs in Europe [1]. Meanwhile, the increasing proportion of stochastic renewable generation in the power grid causes increasing regulation duties for conventional generation assets, including HPPs. Excessive regulation duties are a concern for HPP operators because they lead to increased wear and tear, ultimately shortening service life and requiring expensive maintenance. The need to counteract these effects has been very recently recognized in funded research projects (e.g., [2]) and addressed in recent technical literature. E.g., work [3] has shown that medium-head HPPs providing ancillary services incur in larger penstock fatigue, and authors of [4] proposed a method to reduce it. As an alternative to extending regulation duties of HPPs, the use of batteries was proposed in so-called hybrid HPPs to increment the regulation capacity, e.g., [5].

Conventional HPP regulation loops include the droop governors for primary frequency regulation, the speed changer for secondary frequency control, and the turbine governor. The governor parameters are typically tuned to deliver the design performance (e.g., response time and droop) while respecting the plant's static mechanical and power limits. These classical feedback control loops do not model dynamic mechanical loads explicitly, so they are unaware of possible wear and tear effects that excessive regulation causes. Modeling the

mechanical stress is relevant not only for wear and tear but also to design stress-informed splitting policies for the control signal in plants with multiple controllable elements, like hybrid HPPs.

An alternative to classical regulation loops to develop informed control decisions is model predictive control (MPC), which uses models to formulate constraints explicitly, as for example done in [6] for battery systems using linear prediction models of the battery voltage. In this spirit, this paper proposes linear models of the HPP that can be implemented into an MPC problem to formulate suitable operational constraints of the plant. Two linear models are proposed: a guide vane-to-torque model (key to model the plant's power output) and a guide vane-to-head model, which is essential to characterize mechanical loads and fatigue. By virtue of their linearity, the models allow for a tractable formulation of the MPC problem through convex optimization. These models contribute to advancing the state-of-the-art because typical HPP models for control applications are non-linear transfer-function models (e.g., [7]).

The rest of this paper is organized as follows: Section II describes HPP models, Section III describes the proposed linearization procedures, Section IV the methods for the performance evaluation, Section V presents the results and Section VI draws the main conclusions.

## II. MODELLING HYDROPOWER PLANTS

From a modelling perspective, HPPs feature two main components: hydraulic circuits and turbine, as described next.

### A. Hydraulic circuits

The hydraulic circuit of an HPP consists of the low-pressure tunnel, the penstock, and, in medium- and high-head plants, surge tanks. The penstock is the key element for dynamics because it is subject to the elastic behavior of the water. Its model is described next. The model of the surge tank can be derived by applying the same equivalent circuit principles described here and is not addressed in this paper for a reason of space. The penstock is a pipe that guides water running from upstream to the hydraulic turbine. The water's potential difference between the penstock's inlet and outlet is the source for the mechanical power. The penstock is not open to the air and is subject to water pressure. For this reason, water

This research was supported by the European Union Horizon 2020 research and innovation program in the context of the Hydropower Extending Power System Flexibility project (XFLEX HYDRO, grant agreement No 857832).

elasticity is accounted for in its model. Assuming that the penstock is significantly longer than larger, it can be modeled with a one-dimensional approach using partial differential equations (PDEs), e.g., [8]. PDEs are solved numerically by discretizing the penstock (Fig. 1) into a finite number of elements,  $n$ , of length  $dx = l/n$ , where  $l$  is the total length of the penstock.

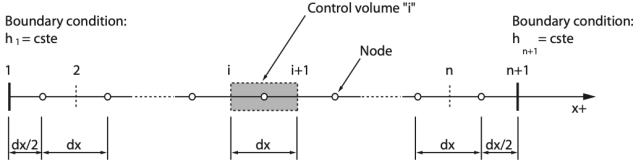


Fig. 1. Spatial discretization of a pipe of length  $L$  [8].

This model can be conveniently visualized and solved in terms of its equivalent circuit model, where each element in Fig. 1 correspond to a (nonlinear) RLC circuit. The relationship between the discharge  $Q_i$  of each penstock element  $i$  and its head  $h_i$  is:

$$\frac{dQ_i}{dt} = -\frac{R(Q_i)}{L} \cdot Q_i - \frac{2}{L} \cdot h_{i+1/2} + \frac{2}{L} \cdot h_i \quad (1a)$$

$$\frac{dQ_{i+1}}{dt} = -\frac{R(Q_i)}{L} \cdot Q_{i+1} + \frac{2}{L} \cdot h_{i+1/2} - \frac{2}{L} \cdot h_{i+1} \quad (1b)$$

$$\frac{dh_{i+1/2}}{dt} = \frac{1}{C} \cdot (Q_i - Q_{i+1}). \quad (1c)$$

where the circuit parameters are

$$R(Q_i) = \frac{\lambda \cdot |Q_i| \cdot dx}{2g \cdot D \cdot A^2}, \quad L = \frac{dx}{g \cdot A}, \quad C = \frac{g \cdot A \cdot dx}{a^2}, \quad (1d)$$

with  $\lambda$  as the Darcy-Weisbach friction coefficient,  $g$  acceleration of gravity,  $A$  pipe cross-section,  $D$  pipe diameter, and  $a$  the wave speed in meters per second (m/s).

The equivalent circuit of a 1-element penstock model is shown in Fig. 3(b) and will be discussed later in combination with the turbine model. The number of penstock elements  $n$  is chosen as a trade-off between computational complexity and modeling accuracy.

## B. Hydraulic turbines

For dynamic power grid simulations, hydraulic turbines are typically modelled using the “quasi-static” approach, which assumes that the behavior of the hydraulic machines can be simulated as a succession of different steady-state conditions during the transition between different operating points [9]. This approach, which preserves acceptable accuracy levels to model dynamic interactions with the power grid and is computationally tractable [8], consists in using characteristic curves, typically determined experimentally, to link all operational variables of a turbine, namely its torque  $T_t$ , rotational speed  $N$ , head  $H_t$ , and flow  $Q_t$ . The characteristic curves are formulated in terms of the so-called unit variables:

$$N_{11} = \frac{N \cdot D_n}{\sqrt{H_t}}, \quad Q_{11} = \frac{Q_t}{D_n^2 \sqrt{H_t}}, \quad T_{11} = \frac{T_t}{D_n^2 H_t} \quad (2)$$

where  $D_n$  is the diameter of the turbine. There are two characteristic curves, one for express the discharge factor  $Q_{11}$ , and the other for the torque factor  $T_{11}$ . Both are a function of the speed factor  $N_{11}$  and the controllable inputs, which are, for Francis turbines, the guide vane  $y$ , and, for Kaplan turbines, the guide vane  $y$  and the blade pitch  $\beta$ .

1) *Francis turbine*: As characteristic curves have typically an “S” shape, a change of variables is typically performed to avoid numerical issues [10]. This consists in defining a polar angle

$$\theta(Q_t, N_t) = \arctan\left(\frac{Q_{11}/Q'_{11}}{N_{11}/N'_{11}}\right) = \arctan\left(\frac{Q_t}{N_t}\right), \quad (3a)$$

and two new functions of  $\theta$  and guide vane  $y$  defined as

$$W_H(\theta, y) = \frac{H_t/H'_t}{(Q_t/Q'_t)^2 + (N/N')^2} \quad (3b)$$

$$W_B(\theta, y) = \frac{T_t/T_n}{(Q_t/Q'_t)^2 + (N/N')^2}, \quad (3c)$$

where  $'$  quantities are values at the best efficiency point. An example of these transformed characteristic curves are shown in Fig. 2 and are the basis to derive the numerical first-order approximations for the linearized models.

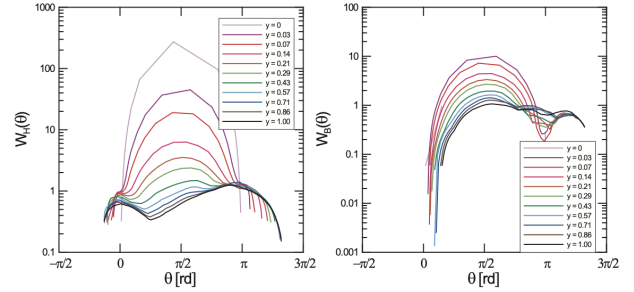


Fig. 2. Polar representation of a Francis characteristic curves [8].

2) *Kaplan turbine*: Kaplan turbines feature a double control system comprising the guide vanes and mobile blades. Compared to the Francis turbine discussed above, their characteristic curves  $W_H(\cdot), W_B(\cdot)$  are a function of the pitch angle  $\beta$ , too.

## C. Complete plant model

The models of the hydraulic circuit and turbine can be combined in an equivalent circuit model [11], as shown in Fig. 3(b), where the RLC circuit refers to the (1-element) penstock and the variable voltage source  $H_t$  to the turbine<sup>1</sup>, modelled with (3b). The inertia of the water and the no-discharge condition at guide vane full closure can be modelled with an equivalent inductance and a resistance in series to the turbine model, respectively [12] - not shown in Fig. 3 for a reason of space. It is convenient to write the equivalent circuit model in its state-space form to visualize all the involved quantities. The (augmented) state-space model also includes

<sup>1</sup>In equivalent circuit models, voltages are analogous to pressures (or heads), and electric currents to the water flow.

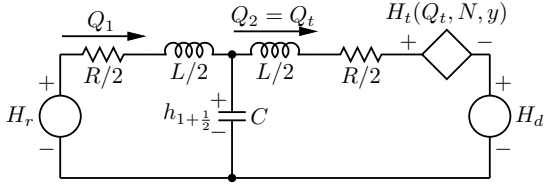


Fig. 3. Equivalent model of hydraulic circuits (with a 1-element penstock) and turbine.

the rotational speed of the machine from Newton's second law for rotation. From the circuit with the 1-element penstock and Francis turbine of Fig. 3(b), the state vector is:

$$x = [Q_1 \quad Q_t \quad h_{1+1/2} \quad \omega]^\top \quad (4a)$$

where  $Q_1$  is the water flow in the penstock's first element,  $Q_t$  is the turbine discharge, and  $\omega$  the turbine angular velocity. The input vector is:

$$u(Q_t, N, y) = \begin{bmatrix} H_r \\ H_t(Q_t, N, y) - H_d \\ T_t(Q_t, N, y) - T_{el} \end{bmatrix} \quad (4b)$$

where  $H_r$  is the reservoir head,  $H_d$  the downstream head,  $T_{el}$  the electrical torque of the generator,  $H_t$  and  $T_{el}$  the turbine head and hydraulic torque from the characteristic curves in (3), and  $^\top$  denotes transpose. They both depend on the state components  $Q_t$  and  $N_t$ , and guide vane opening  $y$ . The (nonlinear) state-space model is:

$$\dot{x} = A(Q_i)x + Bu(Q_t, N, y). \quad (4c)$$

The state and input transformation matrices are:

$$A(x) = \begin{bmatrix} \frac{R(Q_1)}{L} & 0 & -\frac{2}{L} & 0 \\ 0 & \frac{R(Q_t)}{L} & \frac{2}{L} & 0 \\ \frac{1}{C} & -\frac{1}{C} & 0 & 0 \\ 0 & 0 & 0 & 0 \end{bmatrix}, B = \begin{bmatrix} \frac{2}{L} & 0 & 0 \\ 0 & -\frac{2}{L} & 0 \\ 0 & 0 & 0 \\ 0 & 0 & \frac{1}{J} \end{bmatrix} \quad (4d)$$

where  $J$  is the turbine inertia.  $A$  depends on the flow in the penstock and turbine discharge because of the dependency of the hydroacoustic resistance (1d) on the flow.

When the penstock is modelled with  $n$  elements, the state vector has  $(2n+2)$  elements (i.e.,  $n+1$  discharges,  $n$  heads, and 1 rotational speed). The model for the Kaplan turbine includes the dependency of  $H_t$  and  $T_t$  on blade angle  $\beta$ .

### III. LINEAR MODELS

The state-space model in (4) is non-linear in the state and in the controllable input, namely  $y$  for the Francis turbine, and  $y$  and  $\beta$  for the Kaplan. We discuss in this section suitable methods and approximations to derive linearized models, whose performance are then investigated in the results section. The first non-linearity is the dependency between the hydroacoustic resistance  $R$  and the discharge  $Q$  in (1d). By assuming small variations of the operating point (and thus of the discharge),  $R$  can be approximated as a constant value, finally leading to a linear and time-invariant formulation of

the penstock model. The second non-linearity is the turbine's characteristic curves. As turbine models are derived from experimental measurements, a closed-form linearization is not possible, thus we proceed with a numerical linearization of the characteristic curves based on a first-order Taylor expansion, as discussed next.

#### A. Linear model of a Francis turbine

A relation between the head, denoted by  $H_t(Q_t, N, y)$ , and the numerical characteristic curve  $W_h(\cdot)$  is obtained by inverting (3b). The procedure for the torque, not illustrated here, is analogue but considering (3c).

The first-order Taylor expansion of  $H_t(Q_t, N, y)$ , denoted by  $\tilde{H}_t(\cdot)$ , around an operating point with discharge  $Q_{t_0}$ , rotational speed  $N_0$ , and guidevane opening  $y_0$  reads as:

$$\tilde{H}_t(Q_t, N, y) \approx H_t(Q_{t_0}, N_0, y_0) + d_Q^H \cdot (Q_t - Q_{t_0}) + d_N^H \cdot (N - N_0) + d_y^H \cdot (y - y_0). \quad (5)$$

where  $d_Q^H, d_N^H, d_y^H$  are partial derivatives of  $H_t(Q_t, N, y)$  calculated in the operating point. They are computed by differentiating numerically as:

$$d_Q^H := \left. \frac{\partial H_t}{\partial Q_t} \right|_{Q_{t_0}} = \frac{H_t(Q_{t_0} + \epsilon, \cdot) - H_t(Q_{t_0} - \epsilon, \cdot)}{2 \cdot \epsilon}, \quad (6a)$$

$$d_N^H := \left. \frac{\partial H_t}{\partial N} \right|_{N_0} = \frac{H_t(N_0 + \epsilon, \cdot) - H_t(N_0 - \epsilon, \cdot)}{2 \cdot \epsilon}, \quad (6b)$$

$$d_y^H := \left. \frac{\partial H_t}{\partial y} \right|_{y_0} = \frac{H_t(y_0 + \epsilon, \cdot) - H_t(y_0 - \epsilon, \cdot)}{2 \cdot \epsilon}, \quad (6c)$$

where  $\epsilon$  is an arbitrary (small) parameter and  $(\cdot)$  denote the remaining function arguments, kept constant.

#### B. Linearized state-space model

The state-dependant matrix  $A(x)$  in (10d) is calculated for the operating point  $Q_{1_0}$  and  $Q_{t_0}$ , thus resulting in a linear and time-invariant transformation of the state. The next step is expanding the linear models for the turbine head (and torque) in the input vector  $u(\cdot)$  of (10b). The turbine head appears in the second element of the input vector  $u$ ; by using (5), it can be re-written as:

$$H_t(Q_t, N, y) \approx [d_Q^H \quad d_N^H] Mx + d_y^H y + c_H \quad (7a)$$

where  $M$  is a  $2 \times (2 \cdot n + 2)$  matrix such that  $Mx = [Q_t \quad N]^\top$ , and  $c_H$  collects all the known terms of the expression

$$c_H = H_t(Q_{t_0}, N_0, y_0) - d_Q^H Q_{t_0} - d_N^H N_0 - d_y^H y_0 \quad (7b)$$

Similarly, the turbine torque, appearing in the third term of the input vector  $u(\cdot)$  in (10b), can be written as:

$$T_t(Q_t, N, y) \approx [d_Q^T \quad d_N^T] Mx + d_y^T y + c_T \quad (8a)$$

$$c_T = T_t(Q_{t_0}, N_0, y_0) - d_Q^T Q_{t_0} - d_N^T N_0 - d_y^T y_0. \quad (8b)$$

By replacing (7) and (8) in (10b), the state-space in (4c) can be written as:

$$\begin{aligned} \dot{x} = & Ax + B_1 H_r + \\ & + B_2 \cdot \left( \begin{bmatrix} d_Q^H & d_N^H \end{bmatrix} Mx + d_y^H y + c_H - H_d \right) + \\ & + B_3 \cdot \left( \begin{bmatrix} d_Q^T & d_N^T \end{bmatrix} Mx + d_y^T y + c_T - T_{el} \right). \end{aligned} \quad (9)$$

where  $B_1, B_2$  and  $B_3$  are respectively the first, second and third columns of matrix  $B$  in (10d). Eq. (9) can be now written as the following linear state-space

$$\dot{x} = \tilde{A}x + \tilde{B}\tilde{u} \quad (10a)$$

where:

$$\tilde{u} = \begin{bmatrix} H_r & y & (c_H - H_d) & (c_T - T_{el}) \end{bmatrix}^T \quad (10b)$$

$$\tilde{A} = A + B_2 \begin{bmatrix} d_Q^H & d_N^H \end{bmatrix} M + B_3 \begin{bmatrix} d_Q^T & d_N^T \end{bmatrix} M \quad (10c)$$

$$\tilde{B} = \begin{bmatrix} B_1 & (B_2 \cdot d_y^H + B_3 \cdot d_y^T) & B_2 & B_3 \end{bmatrix}. \quad (10d)$$

The state evolution in (10a) is now a linear function of the state and the controllable input, namely the guide vane  $y$ . The input vector (10b) contains, in addition to  $y$ , the reservoir head, the downstream head, electrical torque (these three are input parameters), and constant coefficients  $c_H$  and  $c_T$  that depend on the linearization.

### C. The case of Kaplan turbines

As discussed in Section II-B2, Kaplan turbines can adjust the blade pitch,  $\beta$ , too. The linearization is performed similarly to the Francis turbine, with an additional partial derivative for  $\beta$ . The linear state-space system for the Kaplan,  $\tilde{u}', \tilde{A}', \tilde{B}'$ , is

$$\tilde{u}' = \begin{bmatrix} H_r & y & \beta & (c'_H - H_d) & (c'_T - T_{el}) \end{bmatrix}^T \quad (11a)$$

$$\tilde{A}' = \tilde{A} \quad (11b)$$

$$\tilde{B}' = \begin{bmatrix} B_1 & (B_2 d_y^H + B_3 d_y^T) & (B_2 d_\beta^H + B_3 d_\beta^T) & B_3 \end{bmatrix} \quad (11c)$$

where the known terms contain also the linearization point of the blade pitch  $\beta_0$ :

$$c'_H = c_H - d_\beta^H \beta_0 \quad \text{and} \quad c'_T = c_T - d_\beta^T \beta_0. \quad (11d)$$

## IV. METHODS FOR PERFORMANCE EVALUATION

### A. Case studies

We consider two HPPs of different kind. The first is 87 MW medium-head plant with a Francis turbine. It has a 500 meters penstock and a net head (i.e.,  $H_r - H_d$ ) of 90 meters. The penstock is discretized with  $n = 20$  elements. The second HPP is 39 MW Kaplan low-head unit with a net head of 15m. The short penstock and spiral case is modelled with 8 components.

### B. Procedure to compute the estimation performance

The estimation performance of the linear models is evaluated in time domain simulations by comparing their output against the non-linear models. The procedure to compute the estimation performance is the following:

**(Step 1)** a linear model is computed for each given operating point. The operating point is specified by the guide

vane opening, net head, and rotational speed. Nine different operational points are considered, given by varying the guide vane from 0.2 pu to 1 pu (0 pu and 1 pu represent respectively the all close and all open position), representing the typical operating range of a power plant, with increments of 0.1 pu. The net-head is assumed constant at its nominal value, and the rotational speed at 50 Hz to represent steady-state synchronous operations. For the low-head HPP with Kaplan turbine (that features two regulation mechanisms, guide vane and blade pitch), the pitch is chosen as a function of the guide vane according to the on-cam curve;

**(Step 2)** each linear model is used to simulate operations for a stepwise change of the guide vane. We consider 20 different stepwise changes, from -0.5 pu to 0.5 pu, with increments of 0.025 pu. All the combinations resulting in unfeasible guide vane openings (e.g., guide vane 0.2 and stepwise change of 0.5) are excluded. In this way, a total of 41 x 9 (minus the unfeasible combinations) simulations are performed. For the Kaplan turbine, each guide vane deviation determines a deviation of blade angle according to the on-cam curve.

**(Step 3)** for each simulation, the estimation error is calculated as the difference between the linear model and the ground-truth model.

We analyze estimates of the the turbine torque (relevant in the context of characterizing the mechanical and electric power of the plant) and the spatially averaged head in the penstock for the medium-head HPP, and the head at the turbine for the low-head plant (relevant to asses mechanical load levels, and fatigue, of HPPs).

### C. Performance metrics and notation

We formalize the notions explained in the former section with the objective of defining the metrics. Let  $\Psi$  denote the set with all linearized models of the low-head (or medium-head) HPP, and  $\psi \in \Psi$  a single linearized model. Let set  $X$  denote all possible combinations of linearization points and deviations of guide vane performed in the experiments, where  $\chi \in X$  is a single experiment;  $\hat{y}_T(t, \psi, \chi)$  is a time series that contains the turbine torque of the time-domain simulation of linear model  $\psi$  for experiment  $\chi$ ;  $y_T(t, \chi)$  is the ground-truth time series from the non-linear model for the same experiment. The torque error of linear model  $\psi$  in experiment  $\chi$  is:

$$e_T(t, \psi, \chi) = \frac{y_T(t, \chi) - \hat{y}_T(t, \psi, \chi)}{T_n} \quad (12)$$

where  $T_n$  is the nominal torque. The torque estimation performance is evaluated in terms of the mean absolute error (MAE) of the error  $e$ :

$$\text{MAE} = \sum_{t=t_0}^{t=t_f} |e(t, \psi, \chi)| \quad (13)$$

where the initial and ending time intervals ( $t_0, t_f$ ) are chosen to either capture transient or steady-state conditions. For transient conditions,  $t_0$  corresponds to when the step-wise change is applied and  $t_f = t_0 + 350$  s, where 350 s is determined by empirically by evaluating steady-state conditions ( $\dot{x} \approx 0$ ).

For steady-state conditions,  $t_0$  and  $t_f$  are set to a fixed time interval that correspond to when the system is in steady-state. Head estimations are computed and characterized with the same procedure, scaling the error by the nominal head  $H_n$ .

## V. RESULTS

### A. Medium-head plant with Francis turbine

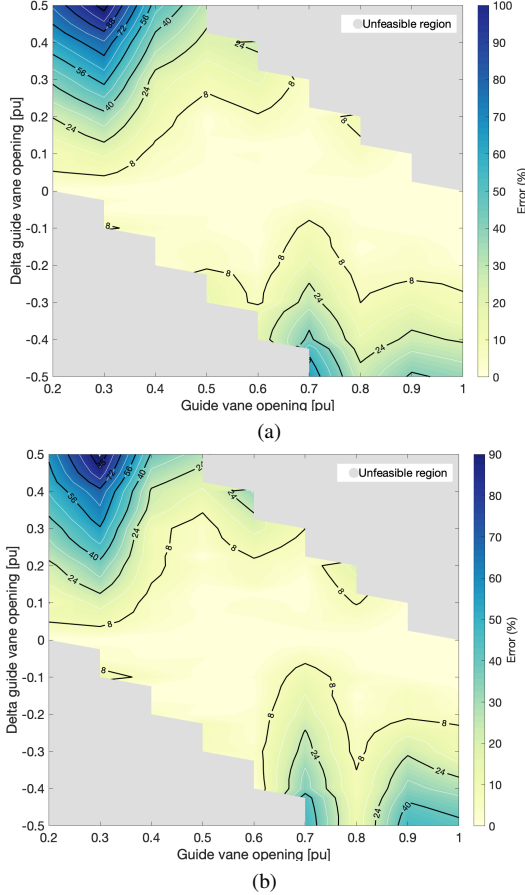


Fig. 4. Francis medium-head HPP, turbine torque: MAE of the linear estimations in transient (a) and steady-state (b) conditions.

Figures 4 and 5 show the transient and steady-state MAE of the torque and head, respectively for the medium-head HPP with Kaplan. The main considerations that can be derived are discussed in the following findings.

**Finding 1:** Linear estimates are more reliable for the head than for the torque. This is due to more prominent non-linearities in the torque model.

**Finding 2:** For a given guide vane opening, estimation performance worsens with larger step-wise variations of the guide vane. This result is to be expected because the linear models are first-order approximations of the nonlinear models; thus, small deviations from the linearization point imply better local approximation.

**Finding 3:** Linear head estimates are better in steady-state (with a maximum error of 1%) than in transient conditions (maximum error: 10%). For the torque, performance is similar in both cases.

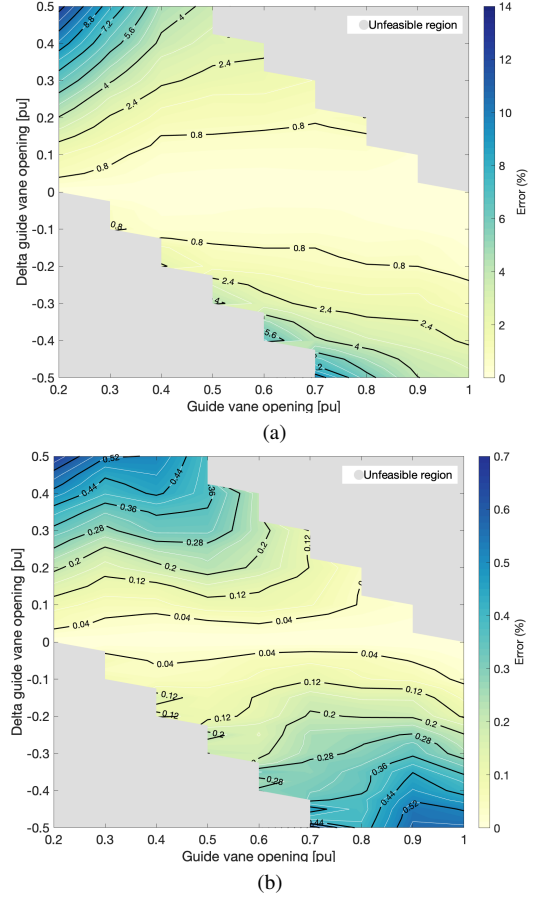


Fig. 5. Francis medium-head HPP, spatially averaged head in the penstock: MAE of the linear estimations in transient (a) and steady-state (b) conditions.

**Finding 4:** For variations of the guide vane smaller than 0.1 pu, torque estimation errors are less than 10% (except for guide vane 0.7 and less than 0.4), and head estimation errors less than 1%.

In the light of Finding 4, it can be concluded that the use of linear models is justified in small-signal applications and where these error levels are acceptable; the advantage is handling computationally tractable models that can be implemented in, for example, (convex) optimization problems for optimal decision-making.

### B. Low-head plant with Kaplan turbine

Transient and steady-state performance of torque and head estimations is respectively shown in figures 6 and 7. Similar observations as for the medium-head HPP can be drawn. In particular: (Finding 1) Linear estimations of the head are more accurate than for torque; (Finding 2) Smaller deviations of stepwise changes result in smaller estimations errors; (Finding 3) head estimates at steady state are significantly more reliable (errors less than 0.1%) than during transients (errors less than 30%). For the torque, there is no significant difference between the two cases; (Finding 4) for small signal variations (e.g.,  $\pm 0.1$  pu of the guidavane), torque errors are approximately within a 10% band, and head errors within 0.8%, thus denoting

relatively small errors of the linear models when used in small-signal applications.

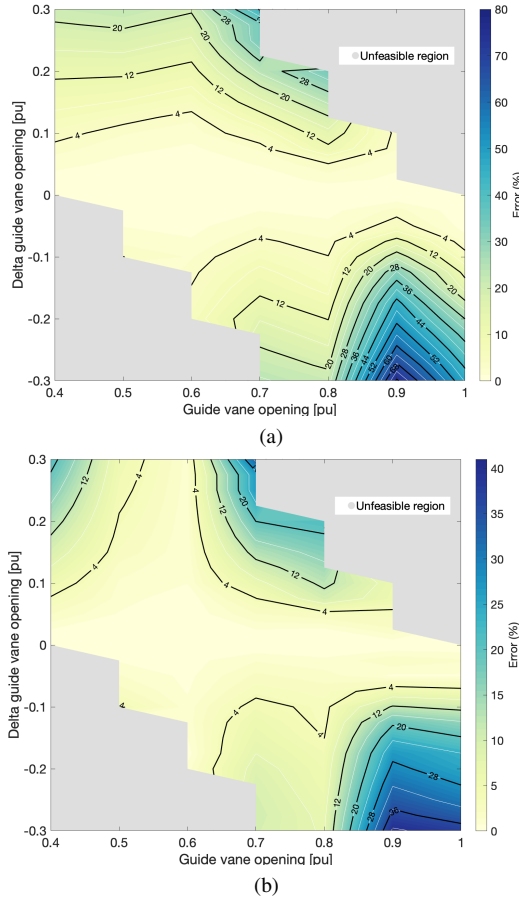


Fig. 6. Kaplan low-head HPP, turbine torque: MAE of the linear estimations in transient (a) and steady-state (b) conditions.

## VI. CONCLUSIONS

This paper presented linearized models of hydropower plants and discussed their performance. The main sources of nonlinearities in both the hydraulic circuit and turbine models were illustrated, and linearization strategies were discussed. Estimation performance was investigated for both medium- and low-head HPPs with Francis and a Kaplan turbine, respectively. Results showed that i) linear estimates of the head are more reliable than for the torque; ii) for variations of the controllable input in a  $\pm 0.1$  pu range, the relative mean absolute error of the linear estimates are less than 10% for the torque and less than 1% for the head. In small signal applications where these error levels are considered acceptable, the linear models are a more tractable alternative to non-linear, opening to the development of efficient model predictive control based on convex optimization.

## REFERENCES

[1] EuroStat, “Electricity generation statistics - first results,” EuroStat, Tech. Rep., 2020. [Online]. Available: <https://ec.europa.eu/eurostat/statistics-explained/pdfscache/9990.pdf>

[2] “Hydropower Extending Power System Flexibility | XFLEX HYDRO Project | H2020 | CORDIS | European Commission.” [Online]. Available: <https://cordis.europa.eu/project/id/857832>

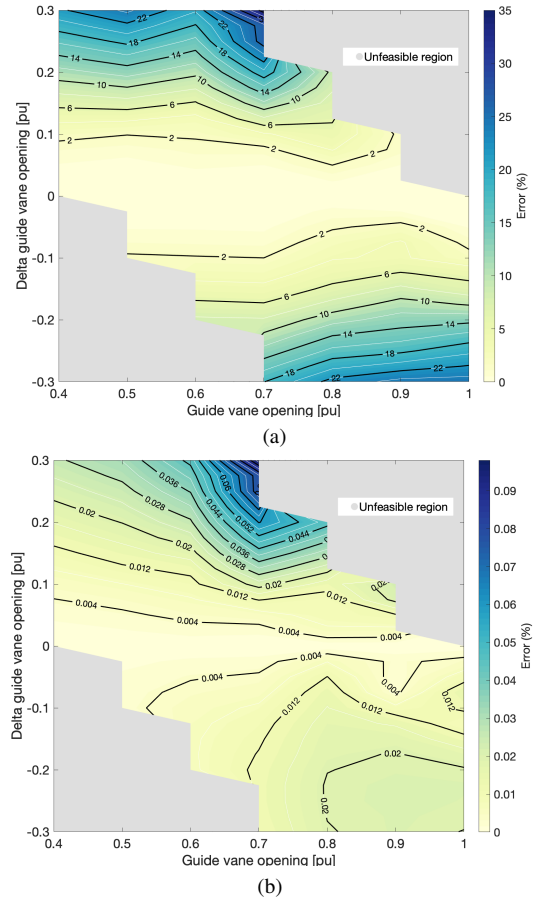


Fig. 7. Kaplan low-head HPP, head at the turbine inlet: MAE linear estimations in transient (a) and steady-state (b) conditions.

[3] M. Dreyer, C. Nicolet, A. Gaspoz, D. Biner, S. Rey-Mermet, C. Saillen, and B. Boulicaut, “Digital clone for penstock fatigue monitoring,” in *IOP Conference Series: Earth and Environmental Science*, vol. 405, no. 1. IOP Publishing, 2019, p. 012013.

[4] S. Cassano, C. Nicolet, and F. Sossan, “Reduction of penstock fatigue in a medium-head hydropower plant providing primary frequency control,” in *2020 55th UPEC*, 2020.

[5] T. Mäkinen, A. Leinonen, and M. Ovakainen, “Modelling and benefits of combined operation of hydropower unit and battery energy storage system on grid primary frequency control,” in *2020 IEEE EEEIC and 2020 IEEE I CPS Europe*, 2020, pp. 1–6.

[6] F. Sossan, E. Namor, R. Cherkaoui, and M. Paolone, “Achieving the dispatchability of distribution feeders through prosumers data driven forecasting and model predictive control of electrochemical storage,” *IEEE Transactions on Sustainable Energy*, vol. 7, 2016.

[7] P. Kundur, “Power system stability,” *Power system stability and control*.

[8] C. Nicolet, “Hydroacoustic modelling and numerical simulation of unsteady operation of hydroelectric systems,” Ph.D. dissertation, EPFL, Lausanne, 2007.

[9] R. Knapp, “Complete characteristics of centrifugal pumps and their use in of transient behavior,” 2014.

[10] M. Marchal, “The calculation of waterhammer problems by means of the digital computer,” *Proc. Intern. Symp. Waterhammer Pumped Storage Projects ASME, 1965-11*, 1965.

[11] O. Jr, N. Barbieri, and A. Santos, “Study of hydraulic transients in hydropower plants through simulation of nonlinear model of penstock and hydraulic turbine model,” *Power Systems, IEEE Transactions on*, vol. 14, pp. 1269 – 1272, 12 1999.

[12] U. Bolleter, E. Buehlmann, J. Eberl, and A. Stirnemann, “Hydraulic and mechanical interactions of feedpump systems. final report,” Electric Power Research Inst., Palo Alto, CA (United States), Tech. Rep., 1992.